

Hip Fracture Risk Assessment Based on Different Failure Criteria Using QCT-Based Finite Element Modeling

Hossein Bisheh^{1,2}, Yunhua Luo^{1,3} and Timon Rabczuk^{4,*}

Abstract: Precise evaluation of hip fracture risk leads to reduce hip fracture occurrence in individuals and assist to check the effect of a treatment. A subject-specific QCT-based finite element model is introduced to evaluate hip fracture risk using the strain energy, von-Mises stress, and von-Mises strain criteria during the single-leg stance and the sideways fall configurations. Choosing a proper failure criterion in hip fracture risk assessment is very important. The aim of this study is to define hip fracture risk index using the strain energy, von Mises stress, and von Mises strain criteria and compare the calculated fracture risk indices using these criteria at the critical regions of the femur. It is found that based on these criteria, the hip fracture risk at the femoral neck and the intertrochanteric region is higher than other parts of the femur, probably due to the larger amount of cancellous bone in these regions. The study results also show that the strain energy criterion gives more reasonable assessment of hip fracture risk based on the bone failure mechanism and the von-Mises strain criterion is more conservative than two other criteria and leads to higher estimate of hip fracture risk indices.

Keywords: Hip fracture risk, finite element model, strain energy, von Mises stress, von Mises strain.

1 Introduction

The most common injury of the elderly during the sideways fall is hip fracture. It was reported that hip fracture may lead to long term disability and death of individuals [Resnick and Greenspan (1989)]. The total number of hip fracture is increasing over the world [Gullberg, Johnell and Kanis (1997)]. Therefore, a special attention must be dedicated on this important issue in order to provide appropriate plans for prevention and treatment of hip fracture. Accurate assessment of hip fracture risk in the elderly helps us to consider proper preventing schemes such as effective design of hip protectors and or providing proper treatment plans to protect the elderly against future hip fracture.

¹ Department of Mechanical Engineering, University of Manitoba, Winnipeg, R3T 5V6, Canada.

² Institute of Structural Mechanics, Bauhaus-Universität Weimar, Weimar, 99423, Germany.

³ Department of Biomedical Engineering, University of Manitoba, Winnipeg, R3T 5V6, Canada.

⁴ Institute of Research and Development, Duy Tan University, Da Nang, Viet Nam.

*Corresponding Author: Timon Rabczuk. Email: Timon.Rabczuk@uni-weimar.de.

Received: 09 December 2019; Accepted: 06 January 2020.

By integrating an imaging technology such as Dual-Energy X-ray Absorptiometry (DXA) or Quantitative Computed Tomography (QCT) and a numerical method such as the finite element (FE) method, a category of more reliable tools for assessing hip fracture risk have been developed which do not have the limitations of statistical models and methods which are based on measuring bone mineral density (BMD). However, in numerical and computational models such as QCT-based finite element models, choosing a proper failure criterion based on the bone microstructure is very important for accurate assessment of hip fracture risk. The human femur consists of inhomogeneous (porous) cancellous bone and nearly homogenous cortical bone, so, their failure mechanism is totally different due to their different microstructures. Failure mechanism of the cancellous bone is often in the form of buckling, and the failure of denser cancellous bone and the cortical bone is mostly characterized by local cracking [Mirzaei, Keshavarzian and Naeini (2014); Stölken and Kinney (2003)]. Although stress- and strain-based failure criteria are accurate for ductile materials such as metal, they may not be accurate for bone because it is categorized as a brittle material [Cordey and Gautier (1999)]. The tensile strength of bone is smaller than their compressive strength, indicating bone should be classified as a brittle material [Cordey and Gautier (1999)]. Due to this property of bone, strain energy criterion which is a combination of both stress and strain effects may lead to more accurate assessment of hip fracture risk. In the literature, hip fracture risk was usually estimated using von Mises stress and von Mises strain criteria [Lotz, Cheal and Hayes (1991); Keyak, Rossi, Jones et al. (1997); Luo, Ferdous and Leslie (2013)], maximum principle stress and strain criteria [Ota, Yamamoto and Morita (1999); Testi, Viceconti, Baruffaldi et al. (1999); Schileo, Taddei, Cristofolini et al. (2008); Gong, Zhang, Fan et al. (2012)], maximum shear stress criterion [Keyak and Rossi (2000)], maximum distortion energy criterion [Keyak and Rossi (2000)], and strain energy criterion [Kheirollahi and Luo (2015); Kheirollahi (2015)]. To the best of our knowledge, there is no comparative study on hip fracture risk assessment by using different failure criteria. The objective of this study is to compare hip fracture risk indices calculated by the strain energy, von Mises stress, and von Mises strain criteria at the critical cross-sections of human femur.

We construct finite element model of the femur from the QCT image of clinical cases and then simulate the single-leg stance and sideways fall configurations by finite element analyses, and finally fracture risk indices are assessed in the critical regions of femur using the strain energy, von Mises stress, and von Mises strain criteria, and then we evaluate and discuss about their rate of conservation and accuracy based on the bone failure mechanism.

2 Methodology

The proposed methodology for assessment of hip fracture risk in the critical regions of femur using the strain energy, von Mises stress, and von Mises strain criteria determined from QCT-based finite element model is shown in Fig. 1. The procedure is explained in detail in the following subsections.

2.1 QCT-Based finite element modeling

2.1.1 QCT scan of femur

To accurate assessment of hip fracture risk, a three-dimensional (3D) finite element model of subject's femur is required. The 3D model is constructed from the QCT image of subject's femur. Thickness of QCT slices is usually considered 1 mm. The QCT images are saved in the Digital Imaging and Communications in Medicine (DICOM) format. To construct a 3D model of a femur, an appropriate segmentation is required to separate the femur from the soft tissue. Each voxel of the QCT image has an intensity defined as Hounsfield Unit (HU), which is associated with bone density [Keyak, Meagher, Skinner et al. (1990); Keaveny, Borchers, Gibson et al. (1993)]. In this study, QCT images of 20 clinical cases, including 10 females and 10 males, were obtained from the Winnipeg Health Science Centre in an anonymous way based on a human research ethics approval. The cases are in the age range of 51 to 78 years (average of 64.5 years). Statistical information of the clinical cases is listed in Tab. 1.

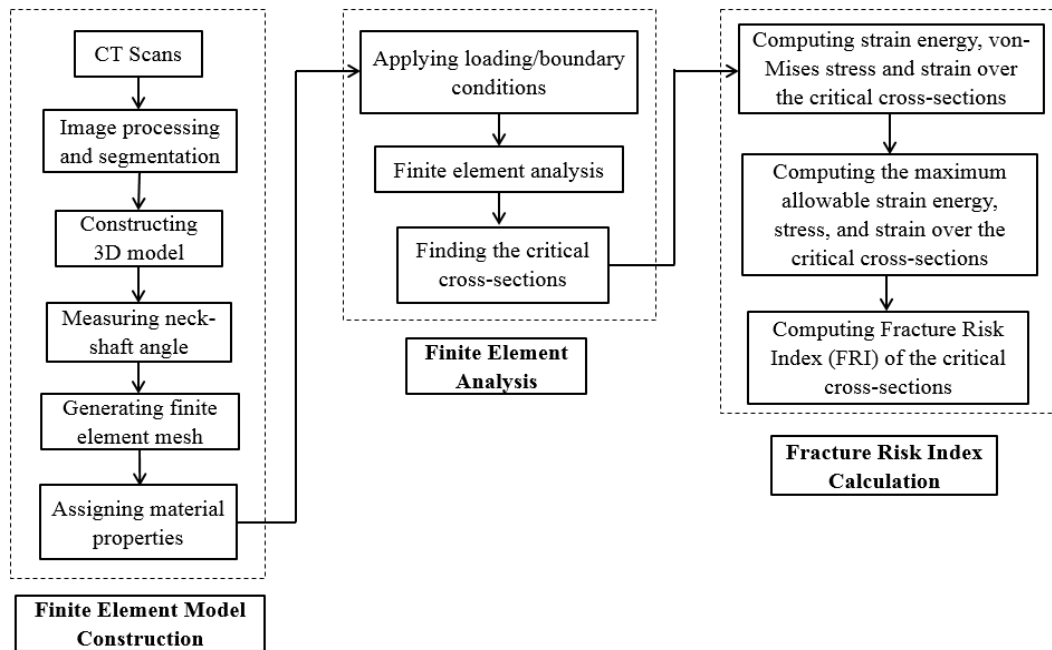


Figure 1: The proposed methodology for calculating hip fracture risk index using the strain energy, von Mises stress, and von Mises strain criteria

Table 1: Statistical information of the 20 clinical cases

	Age (years)	Height (cm)	Body weight (kg)	BMI (kg/m ²)
Range	51-78	155.8-193.2	51.7-111.4	18.83-43.36
Average	64.5	170.33	81.28	28

2.1.2 Generation of finite element mesh

First of all, the 3D model of the femur is constructed from the subject's QCT image using Mimics (Materialise, Leuven, Belgium). QCT images, saved in DICOM format, are imported to Mimics for the required segmentation (Fig. 2(a)) and generation of 3D model of the femur (Fig. 2(b)). Then, a FE mesh is generated by employing the 3-matic module of Mimics (Fig. 2(c)). In this study, the 4-node linear tetrahedral element SOLID72 in ANSYS is utilized. In order to analyze the model convergence, FE models with different maximum element edge lengths are employed. The maximum von Mises stress is obtained for each FE model under the same conditions. The maximum element edge length leading to converged solutions is calculated and utilized in all FE analyses.

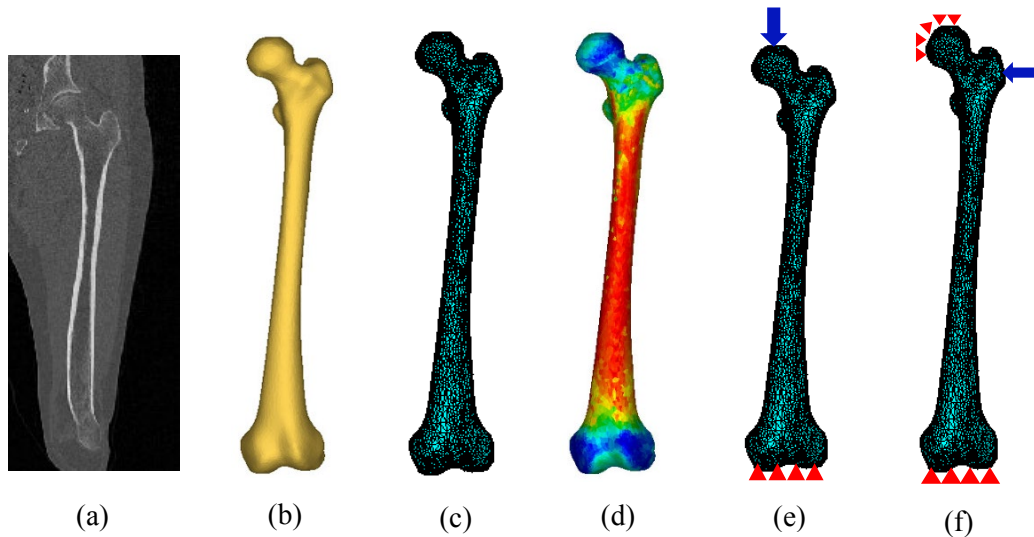


Figure 2: QCT-based finite element analysis of the femur: (a) QCT-scan of the femur; (b) 3D model constructed from the QCT image; (c) 3D finite element model; (d) inhomogeneous isotropic material properties assignment; (e) single-leg stance configuration; and (f) sideways fall configuration. (Color should be used for this figure)

2.1.3 Material properties assignment

To generate a more real FE model, inhomogeneous isotropic material properties are assigned to the femur. The inhomogeneous isotropic mechanical properties of the femur are extracted from the QCT image data using a correlation between the CT numbers and the bone material properties. The bone ash density (ρ_{ash}) is determined according to the

HU number by the following empirical equation [Les, Keyak, Stover et al. (1994); Dragomir-Daescu, Buijs, McEligot et al. (2010)],

$$\rho_{ash} = 0.04162 + 0.000854 HU \quad (\text{g/cm}^3) \quad (1)$$

Eqs. (2)-(4), developed by Keller [Keller (1994)], were used to determine Young's modulus (E), the yield stress (σ_Y), and the yield strain (ε_Y), respectively, according to the bone ash density,

$$E = 10500\rho_{ash}^{2.29} \quad (\text{MPa}) \quad (2)$$

$$\sigma_Y = 116\rho_{ash}^{2.03} \quad (\text{MPa}) \quad (3)$$

$$\varepsilon_Y = 0.011\rho_{ash}^{-0.26} \quad (4)$$

A constant Poisson's ratio ($\nu = 0.4$) is assigned [Keyak, Rossi, Jones et al. (1997); Reilly and Burstein (1975)]. To apply bone material properties, elements are categorized into several discrete material bins using Mimics (Materialise, Leuven, Belgium), representing the continuous distribution of the inhomogeneous bone mechanical properties. A convergence study is fulfilled to determine the required number of material bins. To this purpose, models with different material bins are constructed. The maximum von Mises stress is acquired for each model under the same conditions. The maximum number of material bins generating converged solutions is calculated and employed in all rest simulations. Fig. 2(d) illustrates an isotropic inhomogeneous distribution of bone material properties.

2.2 Finite element analysis

A femur finite element model with the assigned material properties, extracted from Mimics, is imported to ANSYS for further analyses. In finite element analysis, the single-leg stance and sideways fall configurations are simulated. For simulation of the single-leg stance configuration, 2.5 times of the subject's body weight is imposed as a distributed load on the femoral head [Yoshikawa, Turner, Peacock et al. (1994)] and the distal end of the femur is considered completely fixed [Keyak, Rossi, Jones et al. (1997); Bessho, Ohnishi, Matsumoto et al. (2009)] (see Fig. 2(e)),

$$F_{Stance} = 2.5w \quad (\text{N}) \quad (5)$$

where w is the subject's body weight in Newton (N). In sideways fall configuration, the femur is completely fixed at the distal end and the head of femur is fixed in the loading direction (Fig. 2(f)) [Koivumäki, Thevenot, Pulkkinen et al. (2012); Nishiyama, Gilchrist, Guy et al. (2013)]. The representative impact force of sideways fall configuration applying on the greater trochanter (Fig. 2(f)) is given by Yoshikawa et al. [Yoshikawa, Turner, Peacock et al. (1994); Robinovitch, Hayes and McMahon (1991)],

$$F_{Impact} = 8.25w\left(\frac{h}{170}\right)^{\frac{1}{2}} \quad (\text{N}) \quad (6)$$

where h is the height of the subject in centimeter (cm). All loading and boundary conditions are applied to a group of nodes at the greater trochanter, the femoral head, and the distal end of femur (Fig. 2(e) and Fig. 2(f)). All FE simulations are performed automatically using ANSYS Parametric Design Language (APDL) codes. The required solutions for hip fracture risk assessment, including the nodal displacements, stresses, and strains, are obtained from the finite element analysis.

2.3 Critical cross-sections of femur

Three major types of hip fractures are: femoral neck fracture, intertrochanteric fracture, and subtrochanteric fracture (Fig. 3). The intertrochanteric, femoral neck, and subtrochanteric fractures constitute 49, 37, and 14 percent of the total hip fractures, respectively [Michelson, Myers, Jinnah et al. (1995)]. Thus, three critical cross-sections of femur are the smallest femoral neck cross-section (SFN CS), the intertrochanteric cross-section (IntT CS), and the subtrochanteric cross-section (SubT CS) which commonly have the highest fracture risk (Fig. 3). In this study, we determine these critical cross-sections based on the method proposed in the literature [Kheirollahi and Luo (2015); Kheirollahi and Luo (2017)].

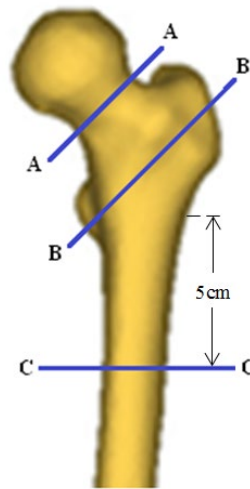


Figure 3: Critical femoral cross-sections: the smallest femoral neck cross-section (A-A), the intertrochanteric cross-section (B-B), and the subtrochanteric cross-section (C-C)

2.4 Hip fracture risk index definition

In this section, hip fracture risk index is defined using the strain energy, von Mises stress, and von Mises strain criteria. The strain energy, von Mises stress, and von Mises strain at the three critical cross-sections of the femur induced by the applied forces are computed using in-house developed MATLAB codes and the data extracted by APDL codes from the obtained finite element solutions. The plane boundaries of the three critical cross-sections, extracted from the finite element mesh, are imported to MATLAB to generate a two dimensional (2-D) mesh for calculating the cross-section strain energy, von Mises stress, and von Mises strain. Fig. 4 shows the generated triangle elements over the smallest femoral neck cross-section, the intertrochanteric cross-section, and the subtrochanteric cross-section.

The strain energy, von Mises stress, and von Mises strain at the three critical cross-sections induced by the applied forces are, respectively, the sum of strain energy, the sum of von Mises stress, and the sum of von Mises strain in all triangle elements of the cross-section, i.e.,

$$U = \sum_{i=1}^m U_e \quad (7a)$$

$$\sigma = \sum_{i=1}^m \sigma_e \quad (7b)$$

$$\varepsilon = \sum_{i=1}^m \varepsilon_e \quad (7c)$$

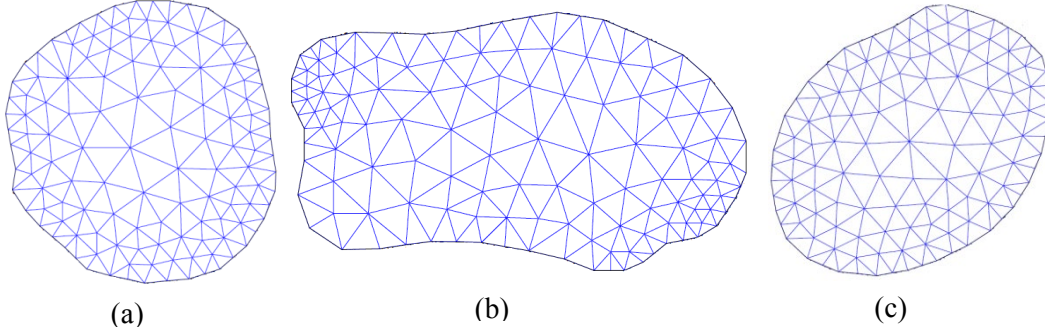


Figure 4: Generated triangle elements over (a) the smallest femoral neck cross-section, (b) the intertrochanteric cross-section, and (c) the subtrochanteric cross-section

where U , σ , and ε are, respectively, the strain energy, von Mises stress, and von Mises strain at the three critical cross-sections of the femur; U_e , σ_e , and ε_e are, respectively, the strain energy, the von Mises stress, and the von Mises strain in a triangle element (e) of the proposed cross-section induced by the applied forces and m is the number of triangle elements created over the proposed cross-sections. Gaussian integration method is used to calculate the strain energy, the von Mises stress, and the von Mises strain in a triangle element (e) of the cross-section. Integration points in each triangle element are determined using in-house MATLAB codes. By using the Gaussian integration method, the strain energy, the von Mises stress, and the von Mises strain of a triangle element (e) induced by the applied forces are calculated as,

$$U_e = \iint \hat{U}_e dA \approx \sum_{i=1}^n W_i |J| \hat{U}_i \quad (8a)$$

$$\sigma_e = \iint \hat{\sigma}_e dA \approx \sum_{i=1}^n W_i |J| \hat{\sigma}_i \quad (8b)$$

$$\varepsilon_e = \iint \hat{\varepsilon}_e dA \approx \sum_{i=1}^n W_i |J| \hat{\varepsilon}_i \quad (8c)$$

where \hat{U}_e , $\hat{\sigma}_e$, and $\hat{\varepsilon}_e$ are, respectively, the strain energy density, the stress, and the strain functions of a triangle element (e); \hat{U}_i , $\hat{\sigma}_i$, and $\hat{\varepsilon}_i$ are, respectively, the strain energy density, the von Mises stress, and the von Mises strain values at the integration points of a triangle element e ; W_i is the weight at the integration points; $|J|$ is determinant of the Jacobean matrix of the triangle element; and n is the number of integration points over the triangle element (integration domain). The von Mises stress and the strain values at the integration points of the triangle elements of the proposed cross-sections are obtained from the results of FE analysis. The strain energy density at an integration point (i) is determined from the finite element solution obtained by the 3D QCT-based FE model, i.e.,

$$\hat{U}_i = \frac{1}{2} \{\sigma\}^T \{\varepsilon\} \quad (9)$$

where $\{\sigma\} = [D]\{\varepsilon\}$ and $\{\varepsilon\} = [B]\{d\}$. The strain energy density at each integration point can be expressed by the finite element solution as,

$$\hat{U}_i = \frac{1}{2} \{d\}_e^T [B]_e^T [D]_e [B]_e \{d\}_e \quad (10)$$

where $\{d\}$ is the displacement vector consisting of displacements at element nodes of the tetrahedral element where the integration point is located; matrix $[B]$ is the derivatives of shape functions of the tetrahedral element; and $[D]$ is the material property matrix of the tetrahedral element,

$$[D]_e = \frac{E}{(1+\nu)(1-2\nu)} \begin{bmatrix} 1-\nu & \nu & \nu & 0 & 0 & 0 \\ \nu & 1-\nu & \nu & 0 & 0 & 0 \\ \nu & \nu & 1-\nu & 0 & 0 & 0 \\ 0 & 0 & 0 & \frac{1}{2}-\nu & 0 & 0 \\ 0 & 0 & 0 & 0 & \frac{1}{2}-\nu & 0 \\ 0 & 0 & 0 & 0 & 0 & \frac{1}{2}-\nu \end{bmatrix} \quad (11)$$

where Poisson's ratio is constant ($\nu = 0.4$) and Young's modulus is function of the bone density obtained from Eq. (2). For each integration point, its Young's modulus is calculated according to the bone density at the point, which is the density of the tetrahedral element where the integration point is located.

The maximum allowable strain energy, stress, and strain of the three critical cross-sections of the femur are also computed using in-house MATLAB codes and the data extracted by APDL codes from the obtained finite element solutions. The maximum allowable strain energy, stress, and strain (or the yield strain energy, yield stress, and yield strain) of the three critical cross-sections are, respectively, the sum of the yield strain energy, the sum of yield stress, and the sum of yield strain in all triangle elements of the cross-section i.e.,

$$U_Y = \sum_{i=1}^m U_Y^e \quad (12a)$$

$$\sigma_Y = \sum_{i=1}^m \sigma_Y^e \quad (12b)$$

$$\varepsilon_Y = \sum_{i=1}^m \varepsilon_Y^e \quad (12c)$$

where U_Y^e , σ_Y^e , and ε_Y^e are, respectively, the yield strain energy, yield stress, and yield strain in a triangle element (e). The Gaussian integration method is also used to calculate the maximum allowable (yield) strain energy, stress, and strain in each triangle element. The maximum allowable strain energy, stress, and strain that a triangle element (e) can sustain are given by,

$$U_Y^e = \iint \hat{U}_Y^e dA \approx \sum_{i=1}^n W_i |J| \hat{U}_{Yi} \quad (13a)$$

$$\sigma_Y^e = \iint \hat{\sigma}_Y^e dA \approx \sum_{i=1}^n W_i |J| \hat{\sigma}_{Yi} \quad (13b)$$

$$\varepsilon_Y^e = \iint \hat{\varepsilon}_Y^e dA \approx \sum_{i=1}^n W_i |J| \hat{\varepsilon}_{Yi} \quad (13c)$$

where \hat{U}_Y^e , $\hat{\sigma}_Y^e$, and $\hat{\varepsilon}_Y^e$ are, respectively, the yield strain energy density, yield stress, and yield strain functions in a triangle element (e); and \hat{U}_{Yi} , $\hat{\sigma}_{Yi}$, and $\hat{\varepsilon}_{Yi}$ are, respectively, the yield strain energy density, yield stress, and yield strain values at the integration points of a triangle element (e) of the proposed cross-section. The yield stress and yield strain of

each integration point is obtained using Eqs. (3) and (4) based on its density, which is the density of the tetrahedral element where the integration point is located. The yield strain energy density at an integration point (i) is calculated as,

$$\hat{U}_{Yi} = \frac{1}{2} \sigma_{Yi} \varepsilon_{Yi} = \frac{\sigma_{Yi}^2}{2E_i} \quad (14)$$

where E_i , σ_{Yi} , and ε_{Yi} are, respectively, the Young's modulus, the yield stress, and the yield strain at the integration point, where all of them are functions of the bone density, which is the density of the tetrahedral element where the integration point is located, as given in Eqs. (2)-(4).

Hip fracture risk index at the three critical cross-sections of the femur using the strain energy, the von Mises stress, and the von Mises strain criteria is defined, respectively, as the ratio of the strain energy, the stress, and the strain induced by the applied forces to the maximum allowable strain energy, stress, and strain of the femur over the proposed cross-sections,

$$\eta = \frac{U}{U_Y} \quad (15a)$$

$$\eta = \frac{\sigma}{\sigma_Y} \quad (15b)$$

$$\eta = \frac{\varepsilon}{\varepsilon_Y} \quad (15c)$$

where η is the fracture risk index at one of the three critical cross-sections of the femur based on the strain energy, the von Mises stress, and the von Mises strain criteria; and U , σ , ε and U_Y , σ_Y , ε_Y are, respectively, obtained from Eqs. (7) and (12).

3 Results

3.1 Convergence studies

3.1.1 Element size in femur finite element analysis

The convergence of finite element solutions in a representative case is shown in Fig. 5. The convergence study shows that the maximum von Mises stress at the narrowest femoral neck converges with the maximum element edge length smaller than 8 mm. Therefore, in construction of the rest of femur FE models, the maximum element edge length is set to 8 mm.

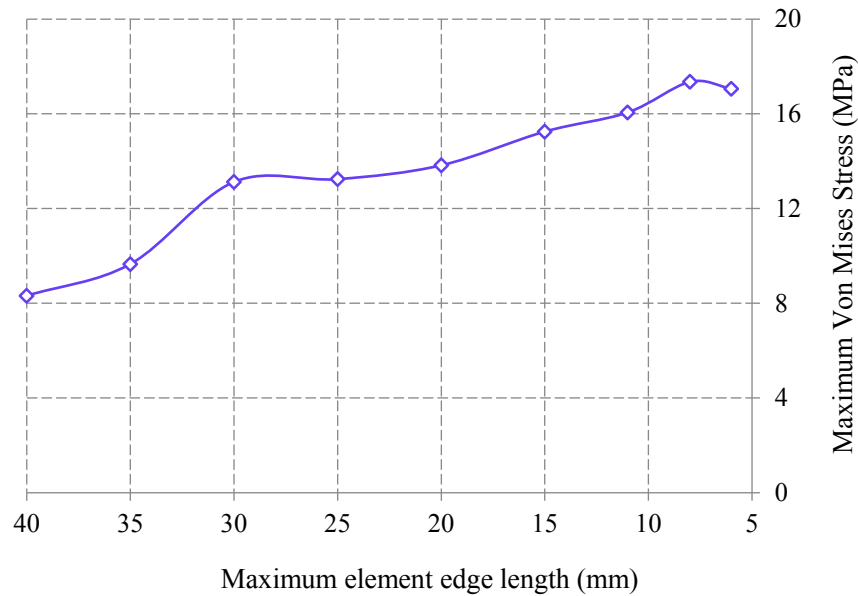


Figure 5: Convergence of the maximum von Mises stress at the femoral neck with element size

3.1.2 Assignment of inhomogeneous material properties

3D femur FE models with different material bins are constructed to investigate model convergence in the inhomogeneous material properties assignment. For each model, the maximum von Mises stress at the narrowest femoral neck is monitored under the same loading and boundary conditions. As shown in Fig. 6, the results of the convergence study indicate that there is no significant change in the maximum von Mises stress with the number of material bins larger than 50. Thus, 50 discrete material bins are considered in the material properties assignment of all cases.

3.1.3 Element size in calculating fracture risk index

Convergence study is also performed to determine the element size used in integrating the cross-sectional strain energy, as it influences on the calculation of fracture risk index (FRI). The FRI at the smallest cross-section of femur is calculated with different maximum element edge lengths. The results are plotted in Fig. 7. The FRI does not change significantly with the maximum element edge length smaller than 5mm. Therefore, the maximum element edge length is set to 5 mm in calculating the cross-sectional strain energy.

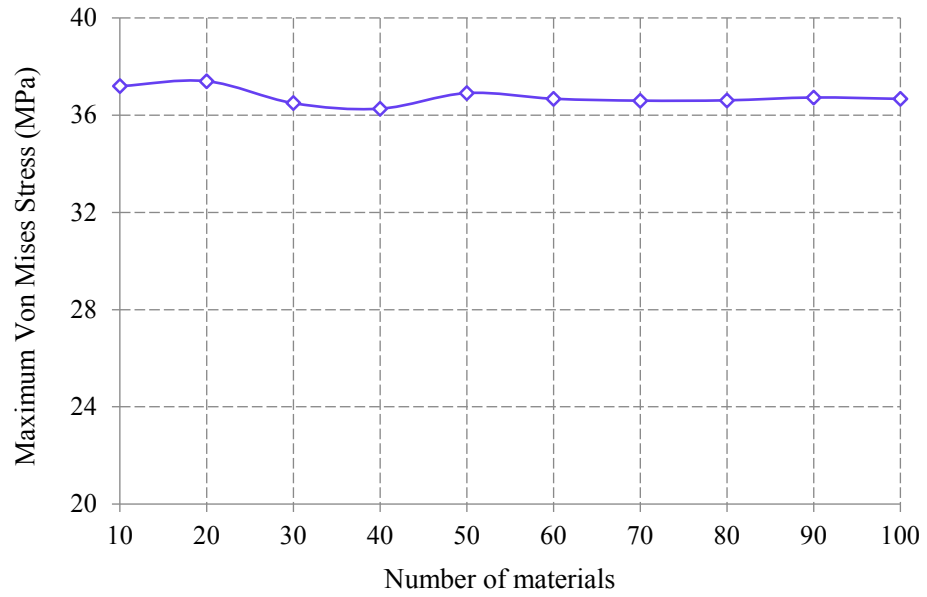


Figure 6: Convergence of the maximum von Mises stress at the femoral neck with the material bins

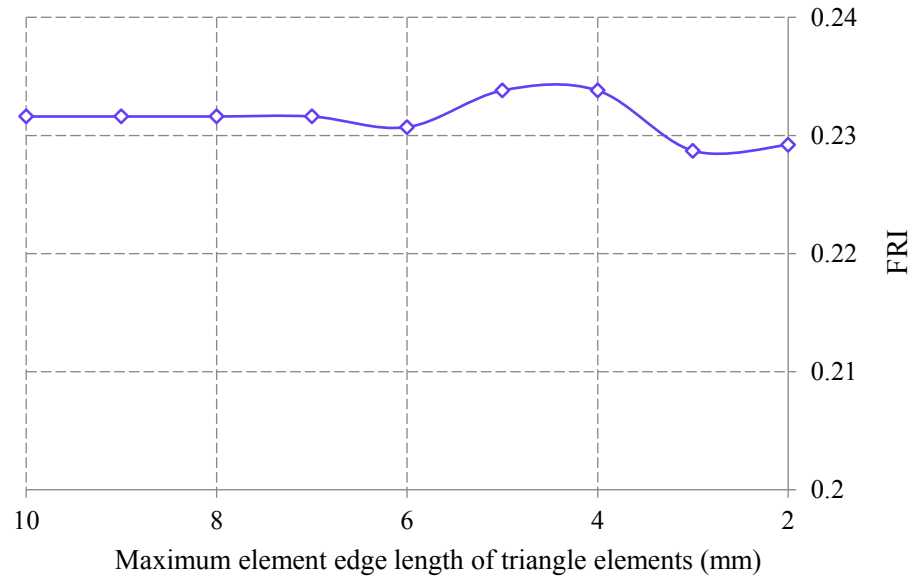


Figure 7: Convergence of the fracture risk index (FRI) with the maximum element edge length of triangle elements generated over the smallest cross-section of femur

3.1.4 Number of integration points in calculating cross-section strain energy, von Mises stress, and von Mises strain

The effect of number of integration points on the calculation of FRI is investigated in this section. FRI at the smallest femoral neck cross-section is computed for 5 clinical cases with different numbers of integration point. The relative errors between FRIs obtained with 3 and 7 integration points are shown in Tab. 2. As it can be seen, the errors are not significant. Therefore, the 3-point integration rule is used in this study to reduce the computational time.

Table 2: Femoral neck FRI obtained with different numbers of integration point

Case No.	FRI		
	3 integration points	7 integration points	Relative error (%)
1	0.239	0.2416	1.07
2	0.6898	0.6975	1.1
3	0.2966	0.2976	0.33
4	0.8885	0.899	1.16
5	1.1482	1.1701	1.87

3.2 Stress and strain patterns at the critical cross-sections

Figs. 8 and 9 show the maximum von Mises stress and von Mises strain at the three critical cross-sections of the femur during both the single-leg stance and the sideways fall for 10 clinical cases including 5 females and 5 males. For the single-leg stance configuration, the patterns in the stresses are different (Tab. 3); first, the differences between the stresses over the three regions are much smaller, and for some cases, the stresses at the subtrochanteric region are higher than those in the other two regions (Fig. 8). The results illustrate that the femoral neck and the intertrochanteric region receive higher stresses than the subtrochanteric region during the sideways fall (Tab. 4). However, strains at the three critical regions of the femur have similar trends in both the single-leg stance and the sideways fall configurations (Tabs. 5 and 6 and Fig. 9).

Table 3: Average maximum von Mises stress (MPa) at the smallest femoral neck cross-section (SFN CS), the intertrochanteric cross-section (IntT CS), and the subtrochanteric cross-section (SubT CS) of the femur for 10 clinical cases during the single-leg stance

	Maximum von Mises stress (MPa)		
	SFN CS	IntT CS	SubT CS
Range	19.56-52.38	23.55-47.8	27.09-43.04
Average	32.93	32.41	35.84

Table 4: Average maximum von Mises stress (MPa) at the smallest femoral neck cross-section (SFN CS), the intertrochanteric cross-section (IntT CS), and the subtrochanteric cross-section (SubT CS) of the femur for 10 clinical cases during the sideways fall

Maximum von Mises stress (MPa)			
	SFN CS	IntT CS	SubT CS
Range	22.78-69.97	16.2-60.3	6.73-33.2
Average	46.52	33.48	18.66

Table 5: Average maximum von Mises strain at the smallest femoral neck cross-section (SFN CS), the intertrochanteric cross-section (IntT CS), and the subtrochanteric cross-section (SubT CS) of the femur for 10 clinical cases during the single-leg stance

Maximum von Mises strain			
	SFN CS	IntT CS	SubT CS
Range	5.25E-03-1.55E-02	5.49E-03-1.87E-02	2.14E-03-4.34E-03
Average	9.55E-03	1.05E-02	3.11E-03

Table 6: Average maximum von Mises strain at the smallest femoral neck cross-section (SFN CS), the intertrochanteric cross-section (IntT CS), and the subtrochanteric cross-section (SubT CS) of the femur for 10 clinical cases during the sideways fall

Maximum von Mises strain			
	SFN CS	IntT CS	SubT CS
Range	1.67E-02-7.43E-02	3.35E-02-1.91E-01	5.08E-04-3.31E-03
Average	4.26E-02	9.37E-02	1.74E-03

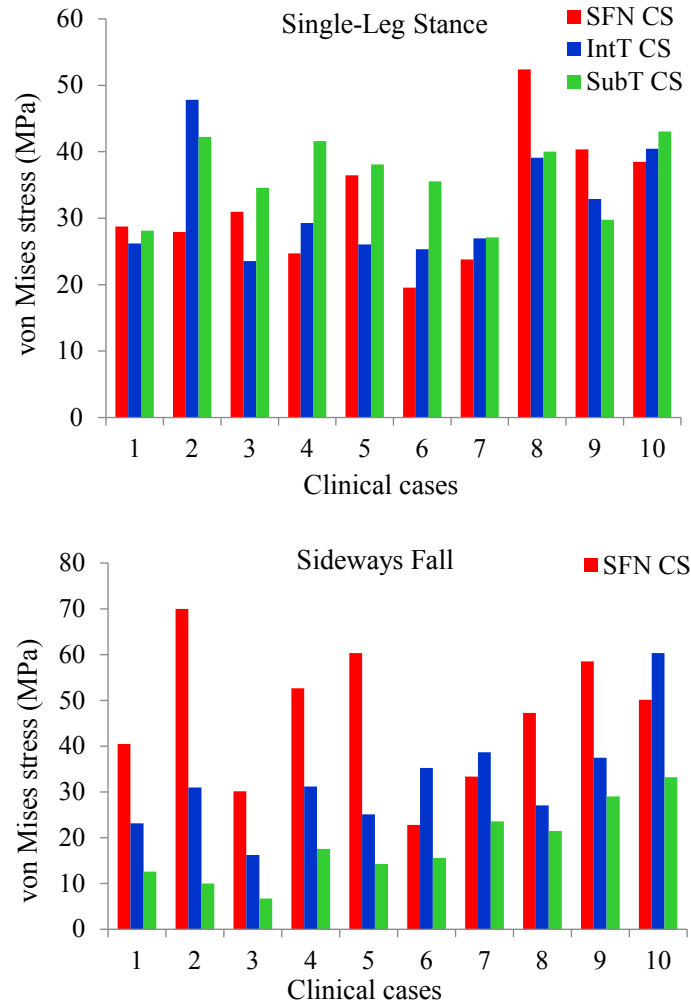


Figure 8: Maximum von Mises stress (MPa) at the smallest femoral neck cross-section (SFN CS), the intertrochanteric cross-section (IntT CS), and the sub-trochanteric cross-section (SubT CS) of the femur for 10 clinical cases during the single-leg stance and the sideways fall. (Color should be used for this figure)

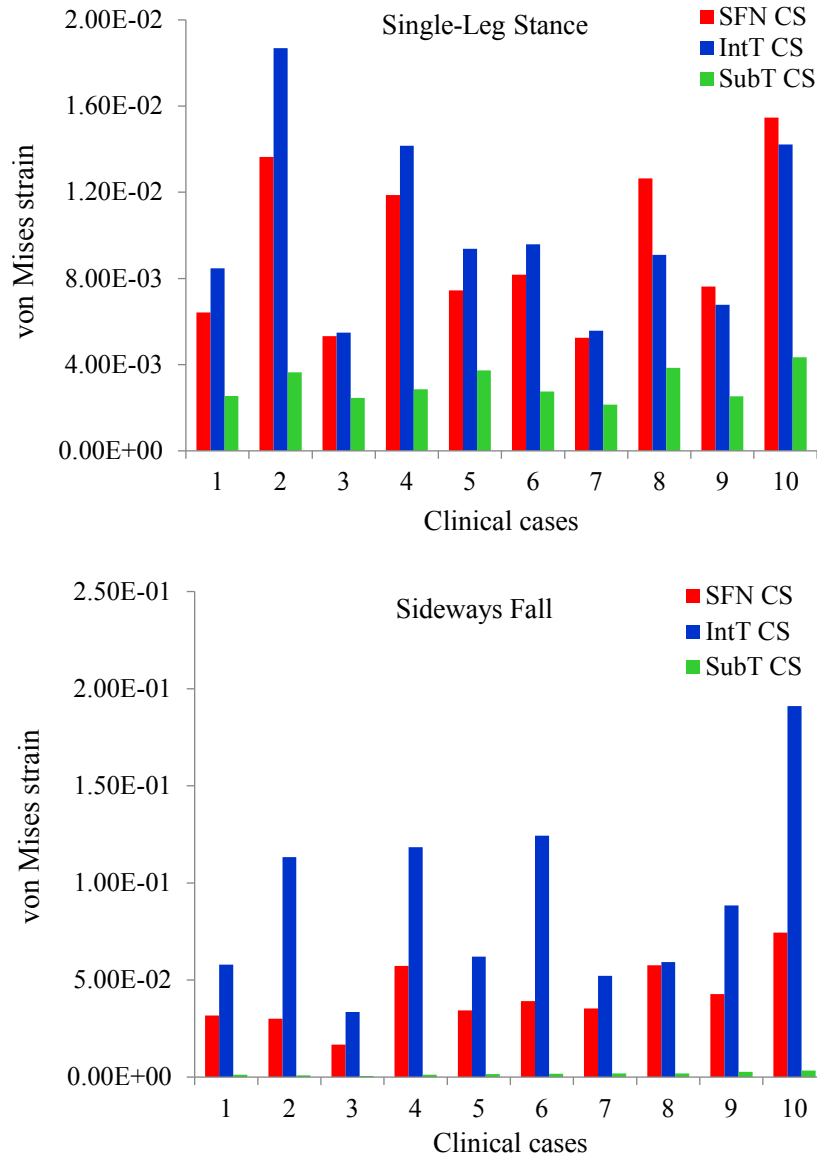


Figure 9: Maximum von-Mises strain at the smallest femoral neck cross-section (SFN CS), the intertrochanteric cross-section (IntT CS), and the sub-trochanteric cross-section (SubT CS) of the femur for 10 clinical cases during the single-leg stance and the sideways fall. (Color should be used for this figure)

3.3 Hip fracture risk indices obtained using the strain energy, von Mises stress, and von Mises strain criteria

For 20 clinical cases (10 females and 10 males), hip fracture risk indices are calculated using the strain energy, von Mises stress, and von Mises strain criteria for the smallest femoral neck, the intertrochanteric, and the subtrochanteric cross-sections of the femur

during the single-leg stance and the sideways fall configurations. The calculated fracture risk indices at the three critical cross-sections of the femur using these three criteria for 10 females and 10 males are shown in Figs. 10-12.

As shown in Figs. 13 and 14, there is not so much difference between the average FRI obtained using the strain energy criterion and that obtained using the von Mises stress criterion for the smallest femoral neck, the intertrochanteric, and the subtrochanteric cross-sections during the sideways fall, however, the average FRI obtained using the strain energy criterion is much higher for these three cross-sections.

During the single-leg stance, as shown in Figs. 10-14, the FRIs obtained using the von Mises stress and von Mises strain criteria are much higher than those obtained using the strain energy criterion. The FRIs obtained using the von Mises stress and von Mises strain criteria during the single-leg stance are to some extent high for a static loading such as stance loading on the femur and they are in the range of the FRIs obtained using the strain energy criterion during the sideways fall. It indicates that based on the von Mises stress and von Mises strain criteria, the elderly are in the risk of hip fracture even during the normal walking. Hence, it is concluded that hip fracture risk assessment using the von Mises stress and von Mises strain criteria is more conservative than hip fracture risk assessment using the strain energy criterion.

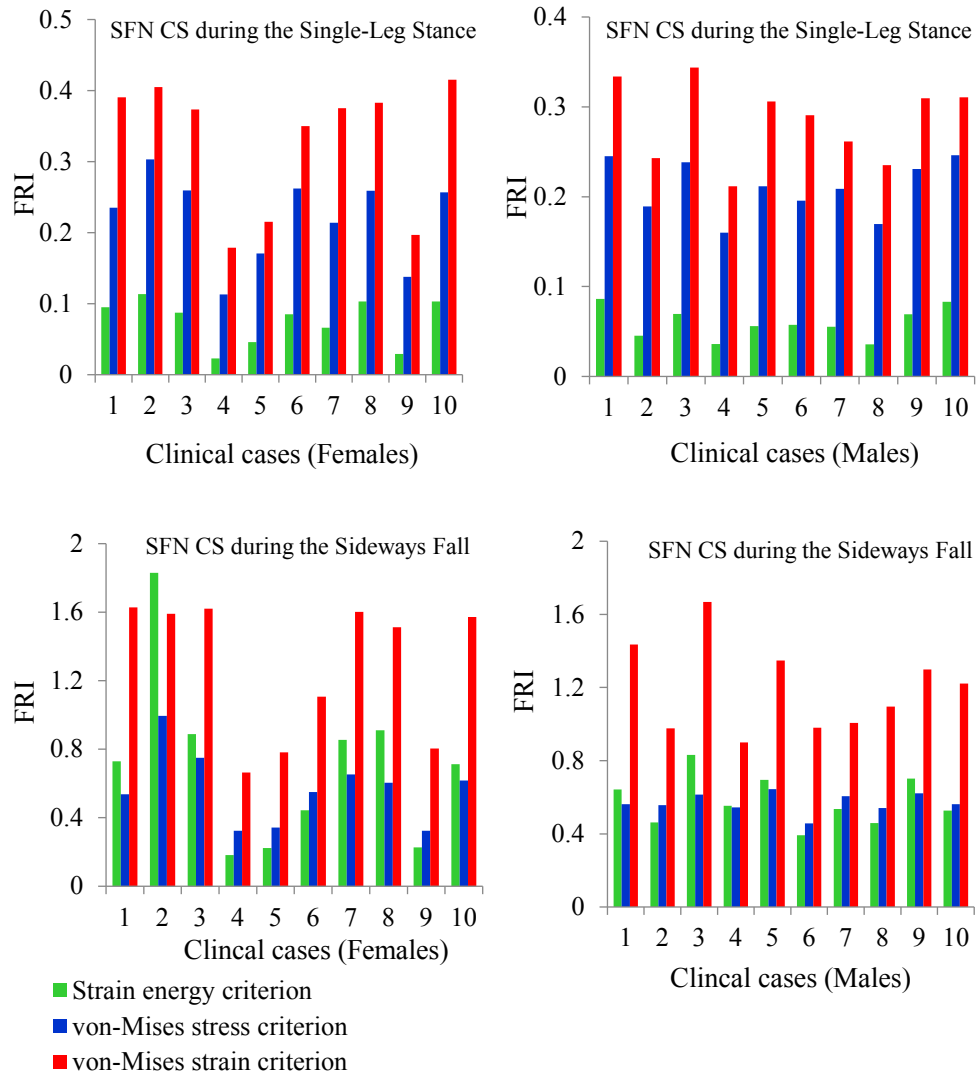


Figure 10: Hip fracture risk index (FRI) at the smallest cross-section of the femoral neck (SFN CS) for 10 females and 10 males during the single-leg stance and the sideways fall configurations using the strain energy, von Mises stress, and von Mises strain criteria. (Color should be used for this figure)

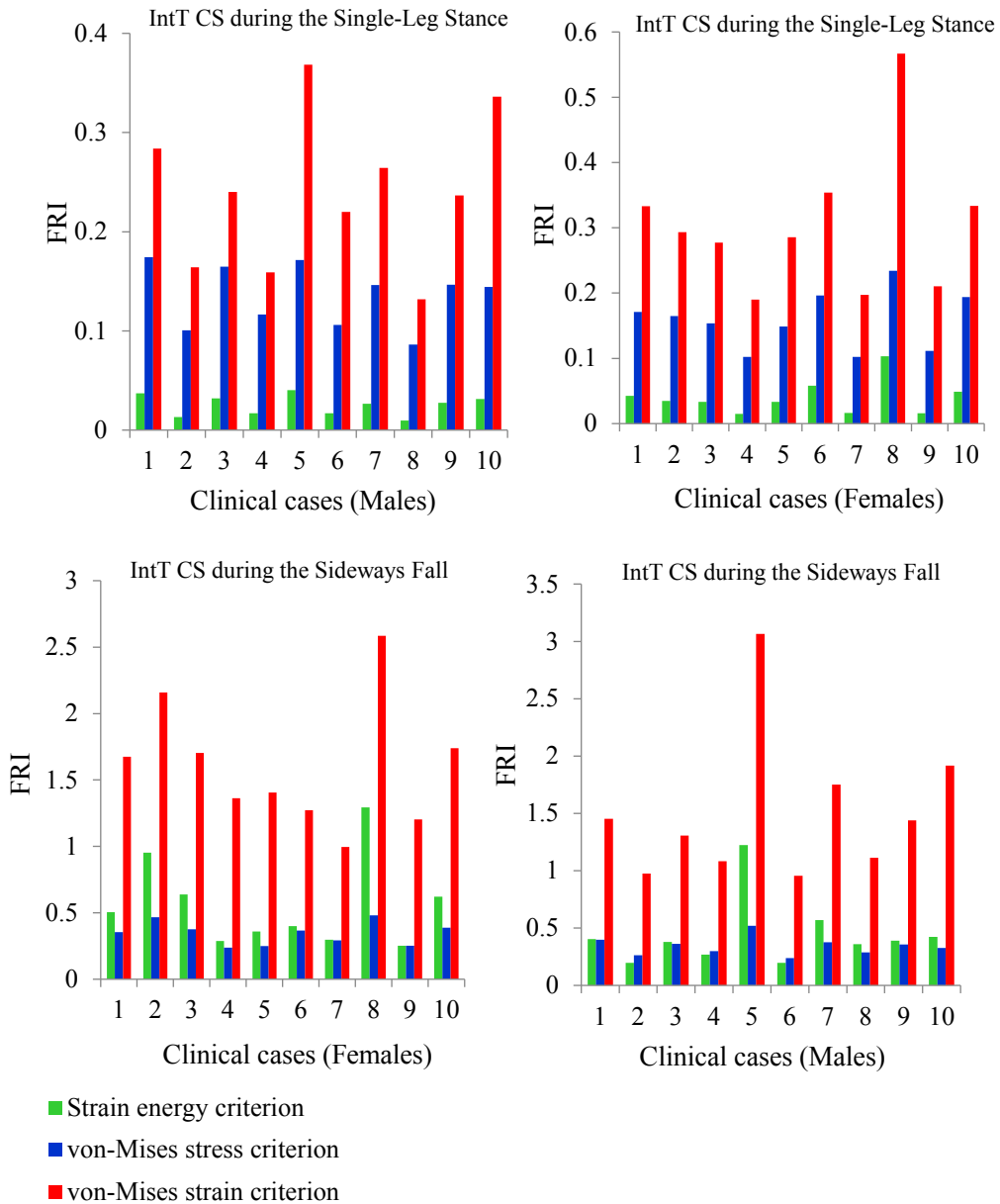


Figure 11: Hip fracture risk index (FRI) at the intertrochanteric cross-section of femur (IntT CS) for 10 females and 10 males during the single-leg stance and the sideways fall configurations using the strain energy, von Mises stress, and von Mises strain criteria. (Color should be used for this figure)

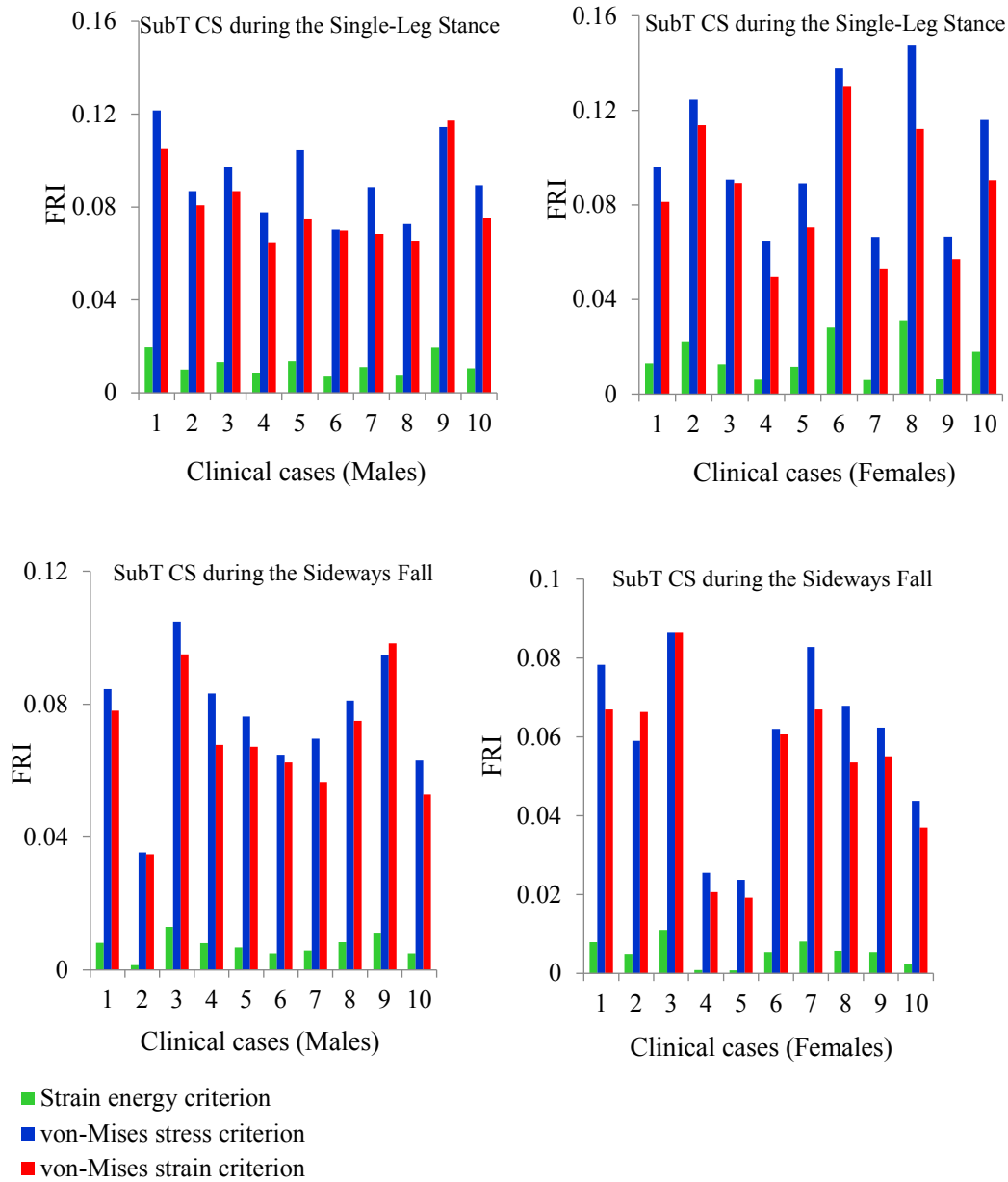


Figure 12: Hip fracture risk index (FRI) at the subtrochanteric cross-section of femur (SubT CS) for 10 females and 10 males during the single-leg stance and the sideways fall configurations using the strain energy, von-Mises stress, and von-Mises strain criteria. (Color should be used for this figure)

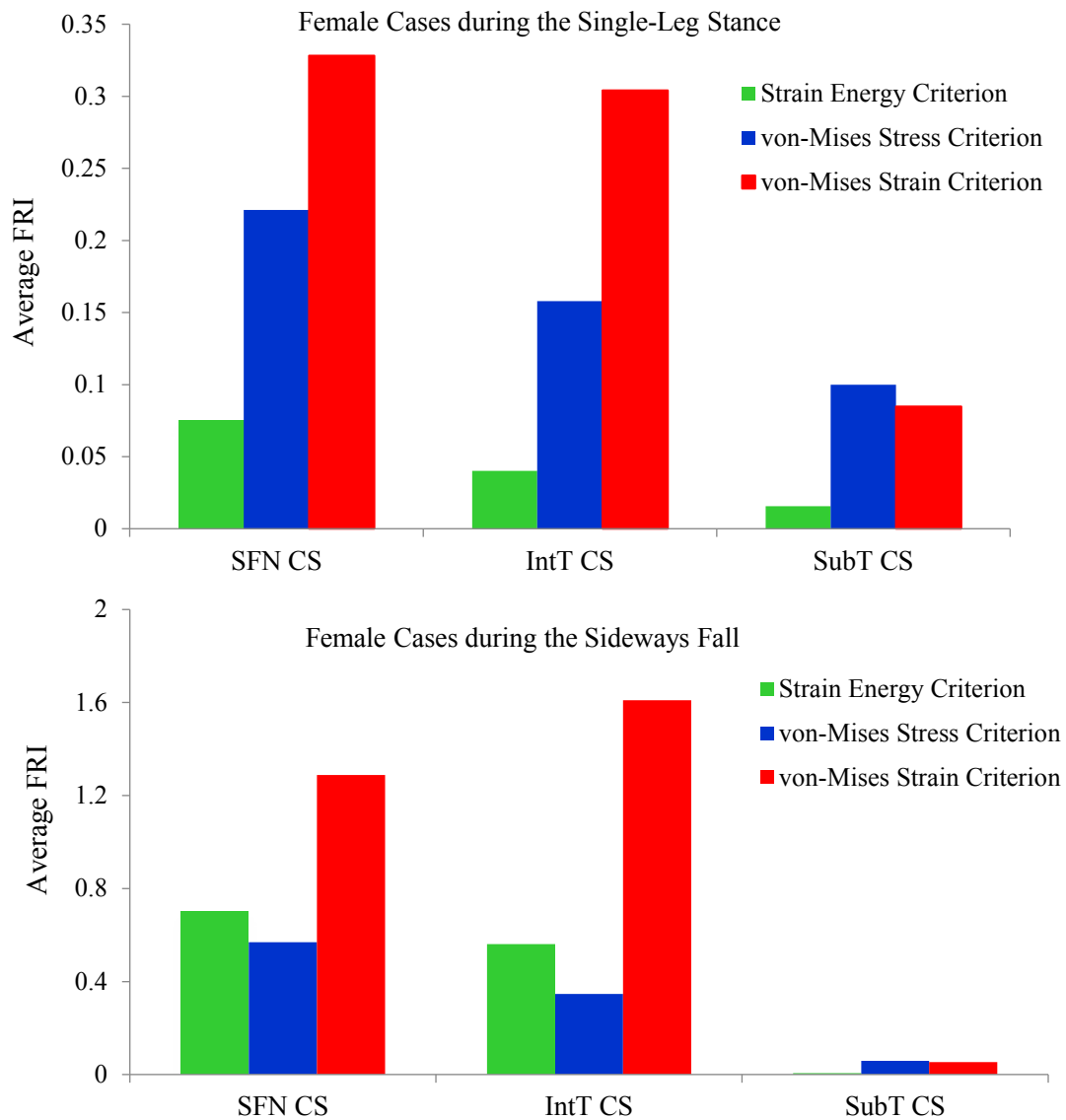


Figure 13: Average FRI at the smallest femoral neck cross-section (SFN CS), the intertrochanteric cross-section (IntT CS), and the subtrochanteric cross-section (SubT CS) of femur for 10 females during the single-leg stance and the sideways fall configurations using the strain energy, von-Mises stress, and von-Mises strain criteria. (Color should be used for this figure)

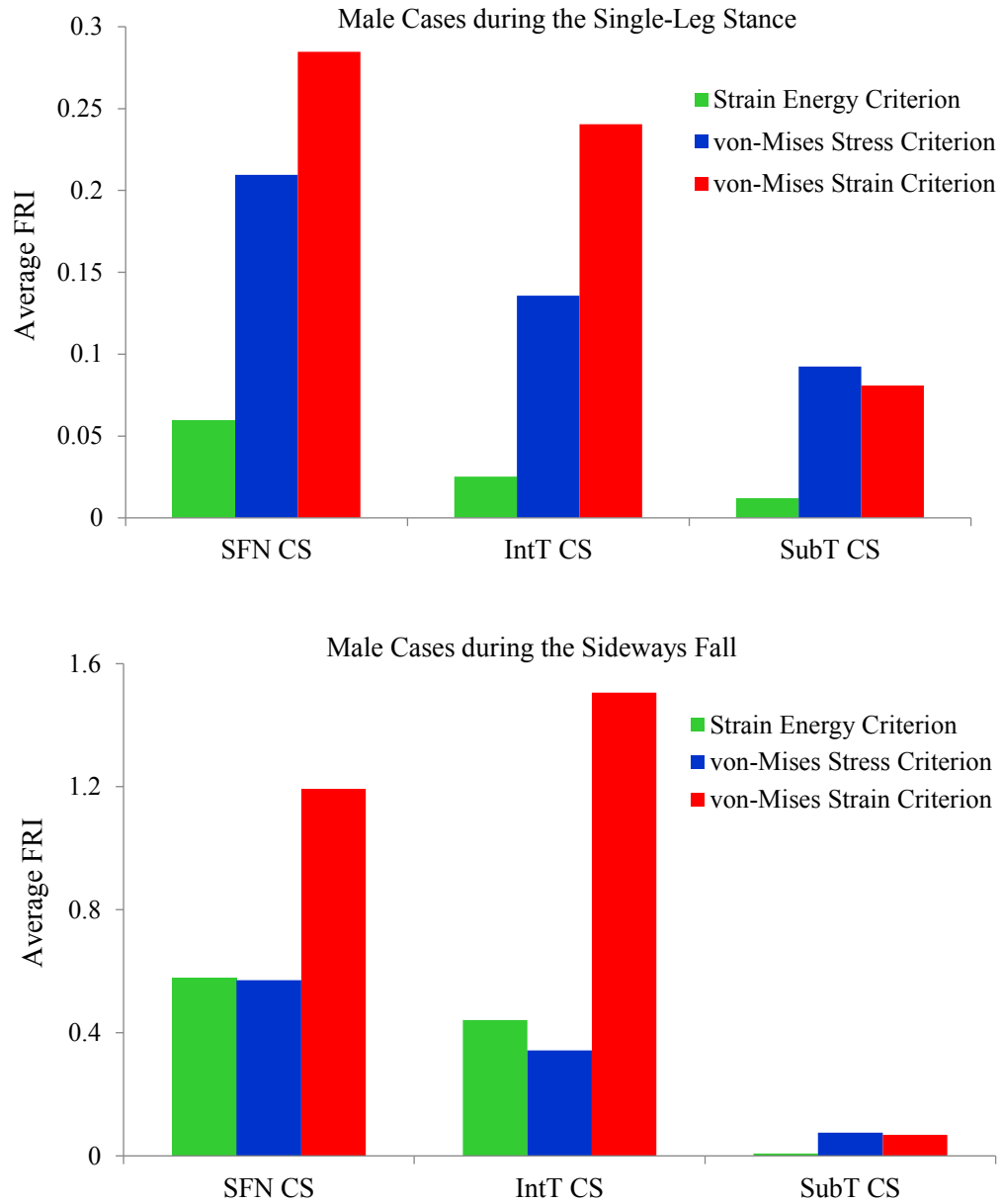


Figure 14: Average FRI at the smallest femoral neck cross-section (SFN CS), the intertrochanteric cross-section (IntT CS), and the subtrochanteric cross-section (SubT CS) of femur for 10 males during the single-leg stance and the sideways fall configurations using the strain energy, von-Mises stress, and von-Mises strain criteria. (Color should be used for this figure)

4 Discussions

Choosing a proper bone failure criterion is challenging. In the literature, stress and strain based failure criteria such as the von Mises stress and von Mises strain criteria and the maximum principle stress and strain criteria were commonly used to assess hip fracture risk. In our previous study [Kheirollahi and Luo (2015)], the strain energy based failure criterion was used for hip fracture risk assessment. Whereas the cancellous bone failure is in the form of buckling and deformation (strain intensity) and the cortical bone failure is related to its local cracking (stress intensity), strain energy failure criterion, which is a combination of both stress and strain intensities, is theoretically more reasonable than other failure criteria for hip fracture risk assessment. There are significant differences between the strains in the three critical regions of the femur during both the single-leg stance and the sideways fall (see Tabs. 5 and 6, and Fig. 9) while the differences between corresponding stresses are not too high (see Tabs. 3 and 4, and Fig. 8), indicating the bone sensitivity with respect to the strains because of its fragility property. Thus, the effects of strains in bone fracture risk assessment have a great importance.

In this study, a comparison has been done between the strain energy, von Mises stress, and von Mises strain criteria on hip fracture risk assessment. The results of the study indicate that for the sideways fall configuration, the von Mises strain criterion gives higher estimate of hip fracture risk indices and is more conservative than the von Mises stress and strain energy criteria in hip fracture risk assessment. While, for the single-leg stance configuration, the von Mises stress and von Mises strain criteria give higher estimate of hip fracture risk with respect to the strain energy criterion and the calculated FRIs using the von Mises stress and von Mises strain criteria for the single-leg stance are in the range of those obtained by the strain energy criterion for the sideways fall configuration. Therefore, based on von Mises stress and von Mises strain criteria, the elderly are in the risk of hip fracture even during the normal walking. However, it can be concluded that the von Mises strain criterion is the most conservative failure criterion in hip fracture risk assessment.

Based on these three failure criteria, the femoral neck and the intertrochanteric region have higher fracture risk than the subtrochanteric region (see Figs. 10-14), which is consistent with the fact that the femoral neck and the intertrochanteric region have a larger proportion of cancellous bone than the subtrochanteric region; and the cancellous bone is generally weaker than the cortical bone. Hence, hip fracture is most likely to initiate first at the femoral neck and then in the intertrochanteric region or in the subtrochanteric region.

Therefore, based on the importance of hip fracture risk assessment and its conservation, the strain energy criterion, the von Mises stress criterion, and or the von Mises strain criterion can be used in evaluation of hip fracture risk in the individuals to consider proper preventive and treatment plans. However, the strain energy criterion can give more reasonable assessment of hip fracture risk based on the bone failure mechanism, because it considers both effects of stress and strain simultaneously.

5 Conclusion

Choosing a reliable failure criterion to assess hip fracture risk in the individuals is

crucially important for preventing hip fracture and initiating a treatment. The purpose of this study is to compare the strain energy, von Mises stress, and von Mises strain criteria in estimation of hip fracture risk. The results of this study show that the strain energy failure criterion leads to more reliable assessment of hip fracture risk than the von Mises stress and von Mises strain criteria. However, the von Mises strain criterion is more conservative than other two criteria. The results of this study can be used in clinical applications to evaluate hip fracture risk and monitor the effects of corresponding treatments, and also in future studies regarding hip fracture risk assessment.

Conflicts of Interest: The authors declare that they have no conflicts of interest to report regarding the present study.

References

- Bessho, M.; Ohnishi, I.; Matsumoto, T.; Ohashi, S.; Matsuyama, J. et al.** (2009): Prediction of proximal femur strength using a CT-based nonlinear finite element method: differences in predicted fracture load and site with changing load and boundary conditions. *Bone*, vol. 45, no. 2, pp. 226-231.
- Cordey, J.; Gautier, E.** (1999): Strain gauges used in the mechanical testing of bones. Part I: theoretical and technical aspects. *Injury*, vol. 30, Supplement 1, pp. SA7-SA13.
- Dragomir-Daescu, D.; Buijs, J. O. D.; McEligot, S.; Dai, Y.; Entwistle, R. C. et al.** (2010): Robust QCT/FEA models of proximal femur stiffness and fracture load during a sideways fall on the hip. *Annals of Biomedical Engineering*, vol. 39, no. 2, pp. 742-755.
- Gong, H.; Zhang, M.; Fan, Y.; Kwok, W. L.; Leung, P. C.** (2012): Relationships between femoral strength evaluated by nonlinear finite element analysis and BMD, material distribution and geometric morphology. *Annals of Biomedical Engineering*, vol. 40, no. 7, pp. 1575-1585.
- Gullberg, B.; Johnell, O.; Kanis, J. A.** (1997): World-wide projections for hip fracture. *Osteoporosis International*, vol. 7, no. 5, pp. 407-413.
- Keaveny, T. M.; Borchers, R. E.; Gibson, L. J.; Hayes, W. C.** (1993): Trabecular bone modulus and strength can depend on specimen geometry. *Journal of Biomechanics*, vol. 26, no. 8, pp. 991-1000.
- Keller, T. S.** (1994): Predicting the compressive mechanical behavior of bone. *Journal of Biomechanics*, vol. 27, no. 9, pp. 1159-1168.
- Keyak, J. H.; Rossi, S. A.; Jones, K. A.; Skinner, H. B.** (1997): Prediction of femoral fracture load using automated finite element modeling. *Journal of Biomechanics*, vol. 31, no. 2, pp. 125-133.
- Keyak, J. H.; Rossi, S. A.** (2000): Prediction of femoral fracture load using finite element models: an examination of stress- and strain-based failure theories. *Journal of Biomechanics*, vol. 33, no. 2, pp. 209-214.
- Keyak, J. H.; Meagher, J. M.; Skinner, H. B.; Mote Jr, C. D.** (1990): Automated three-dimensional finite element modelling of bone: a new method. *Journal of Biomedical Engineering*, vol. 12, no. 5, pp. 389-397.

Kheirollahi, H.; Luo, Y. (2015): Assessment of hip fracture risk using cross-section strain energy determined by QCT-based finite element modeling. *BioMed Research International*, vol. 2015, pp. 1-15.

Kheirollahi, H. (2015): *Assessment of Hip Fracture Risk Using Cross-Section Strain Energy Determined from QCT-Based Finite Element Model (M.Sc. Thesis)*, University of Manitoba, Canada.

Kheirollahi, H.; Luo, Y. (2015): Identification of high stress and strain regions in proximal femur during single-leg stance and sideways fall using QCT-based finite element model. *International Journal of Biomedical and Biological Engineering*, vol. 9, no. 8, pp. 633-640.

Kheirollahi, H.; Luo, Y. (2017): Understanding hip fracture by QCT-based finite element modeling. *Journal of Medical and Biological Engineering*, vol. 37, no. 5, pp. 686-694.

Koivumäki, J. E. M.; Thevenot, J.; Pulkkinen, P.; Kuhn, V.; Link, T. M. et al. (2012): CT-based finite element models can be used to estimate experimentally measured failure loads in the proximal femur. *Bone*, vol. 50, no. 4, pp. 824-829.

Les, C. M.; Keyak, J. H.; Stover, S. M.; Taylor, K. T.; Kaneps, A. J. (1994): Estimation of material properties in the equine metacarpus with use of quantitative computed tomography. *Journal of Orthopaedic Research*, vol. 12, no. 6, pp. 822-833.

Lotz, J. C.; Cheal, E. J.; Hayes, W. C. (1991): Fracture prediction for the proximal femur using finite element models: part I-linear analysis. *Journal of Biomechanical Engineering*, vol. 113, no. 4, pp. 353-360.

Lotz, J. C.; Cheal, E. J.; Hayes, W. C. (1991): Fracture prediction for the proximal femur using finite element models: part II-nonlinear analysis. *Journal of Biomechanical Engineering*, vol. 113, no. 4, pp. 361-365.

Luo, Y.; Ferdous, Z.; Leslie, W. D. (2013): Precision study of DXA-based patient-specific finite element modeling for assessing hip fracture risk. *International Journal for Numerical Methods in Biomedical Engineering*, vol. 29, no. 5, pp. 615-629.

Michelson, J. D.; Myers, A.; Jinnah, R.; Cox, Q.; Van Natta, M. (1995): Epidemiology of hip fractures among the elderly. Risk factors for fracture type. *Clinical Orthopaedics and Related Research*, no. 311, pp. 129-135.

Mirzaei, M.; Keshavarzian, M., Naeini, V. (2014): Analysis of strength and failure pattern of human proximal femur using quantitative computed tomography (QCT)-based finite element method. *Bone*, vol. 64, pp. 108-114.

Nishiyama, K. K.; Gilchrist, S.; Guy, P.; Cripton, P., Boyd, S. K. (2013): Proximal femur bone strength estimated by a computationally fast finite element analysis in a sideways fall configuration. *Journal of Biomechanics*, vol. 46, no. 7, pp. 1231-1236.

Ota, T.; Yamamoto, I.; Morita, R. (1999): Fracture simulation of the femoral bone using the finite-element method: how a fracture initiates and proceeds. *Journal of Bone and Mineral Metabolism*, vol. 17, no. 2, pp. 108-112.

Reilly, D. T.; Burstein, A. H. (1975): The elastic and ultimate properties of compact bone tissue. *Journal of Biomechanics*, vol. 8, no. 6, pp. 393-405.

Resnick, N. M.; Greenspan, S. L. (1989): ‘Senile’ osteoporosis reconsidered. *Journal of the American Medical Association*, vol. 261, no. 7, pp. 1025-1029.

Robinovitch, S. N.; Hayes, W. C.; McMahon, T. A. (1991): Prediction of femoral impact forces in falls on the hip. *Journal of Biomechanical Engineering*, vol. 113, no. 4, pp. 366-374.

Schileo, E.; Taddei, F.; Cristofolini, L.; Viceconti, M. (2008): Subject-specific finite element models implementing a maximum principal strain criterion are able to estimate failure risk and fracture location on human femurs tested *in vitro*. *Journal of Biomechanics*, vol. 41, no. 2, pp. 356-367.

Stölken, J. S.; Kinney, J. H. (2003): On the importance of geometric nonlinearity in finite-element simulations of trabecular bone failure. *Bone*, vol. 33, no. 4, pp. 494-504.

Testi, D.; Viceconti, M.; Baruffaldi, F.; Cappello, A. (1999): Risk of fracture in elderly patients: a new predictive index based on bone mineral density and finite element analysis. *Computer Methods and Programs in Biomedicine*, vol. 60, no. 1, pp. 23-33.

Yoshikawa, T.; Turner, C. H.; Peacock, M.; Slemenda, C. W.; Weaver, C. M. et al. (1994): Geometric structure of the femoral neck measured using dual-energy X-ray absorptiometry. *Journal of Bone and Mineral Research*, vol. 9, no. 7, pp. 1053-1064.